J Mater Sci (2011) 46:910–922
DOI 10.1007/s10853-010-4834-4

Synthesis and structural characterization of Fe^{3+}-doped calcium hydroxyapatites: role of precursors and synthesis method

G. Salviulo · M. Bettinelli · U. Russo · A. Speghini · L. Nodari

Received: 30 April 2010 / Accepted: 14 August 2010 / Published online: 27 August 2010

Abstract This study evaluates the role of Ca and P precursors and of two different preparation methods, ceramic and hydrothermal, in the synthesis of undoped- and Fe^{3+}-doped hydroxyapatite (HA), and tests the Fe^{3+} solubility limits in HA. Previous studies have noted that different synthesis conditions lead to different products in variable amounts and recent literature quotes the highest amount of Fe^{3+} substituting for Ca in the HA structure in the range 0.2–0.5 as a function of temperature. Samples were characterized by X-ray powder diffraction, Mössbauer and Infrared spectroscopies. The samples obtained by the ceramic method at 800 °C contain mixtures of B-type carbonate-apatite and other phosphates whose type and number depend on Ca and P precursors. Samples synthesized at higher temperatures contain mixtures of hydroxyapatite, tricalcium phosphate and of magnetic phases, as haematite and ferrite, whose relative amounts depend on nominal composition and thermal treatment. Samples obtained by a hydrothermal route are richer in HA phase with respect to the solid state one, even if the obtained HA percentage depends on the pH. Mössbauer results suggest that Fe^{3+} is randomly distributed between Ca1 and Ca2 sites. At the highest doping levels a reduction takes place with the formation of iron(II) and magnetite.

G. Salviulo (✉)
Dipartimento di Geoscienze, Università di Padova,
Via Matteotti, 26, 35131 Padova, Italy
e-mail: gabriella.salviulo@unipd.it

M. Bettinelli
Laboratorio di Chimica dello Stato Solido, DB, Università di Verona and INSTM, UdR Verona, Ca' Vignal, Strada Le Grazie 15, 37134 Verona, Italy

U. Russo · L. Nodari
Dipartimento di Scienze Chimiche, Università di Padova and INSTM, UdR Padova, Via Marzolo 1, 35136 Padova, Italy

A. Speghini
DiSTeMeV, Università di Verona and INSTM, UdR Verona, Villa Lebrecht-Via della Pieve, 37029 San Floriano (Verona), Italy

Introduction

Calcium phosphate apatites form a wide class of inorganic crystalline compounds of chemical formula $Ca_{10}(PO_4)_6(OH,F,Cl)_2$. The mineral apatite has a great importance in a large variety of research and applied fields such as Earth science, life science and materials science [1 and references herein reported] because its atomic arrangement allows numerous chemical substitutions for both Ca and (PO_4) groups. Natural apatite is the phosphate most used for the production of fertilizers, detergents and phosphoric acid [2]. Hydroxyapatite is the main mineral constituent of human bones, teeth and many biological calcifications [3]. Synthetic hydroxyapatite (HA) is used as an environmental absorber of metal ions due to its cation-exchange property [4] and as a support for heterogeneous catalysis [5]. In addition HA presents high biocompatibility with natural bones and can be easily incorporated in biological tissues, and so it finds various applications as a bioceramic material [6].

Numerous synthetic methodologies for the preparation of HA are known, such as wet precipitation, solid state synthesis, hydrolysis, hydrothermal and sol–gel methods [6–9]. Previous studies have noted that the solid state syntheses can lead to different product compositions as a consequence of the heating rate, the value of the highest reaction temperature and the permanence time at this temperature, but in the literature there are no data

suggesting the optimal temperature and reaction time. In addition, sintering at elevated temperatures has the tendency to eliminate the functional OH group and results in the decomposition of HA into α-tricalcium phosphate (α-TCP), β-tricalcium phosphate (β-TCP) and tetracalcium phosphate (TTCP) [6].

Numerous cations can substitute for calcium in the structure of hydroxyapatite $Ca_{10}(PO_4)_6(OH)_2$ and their incorporation affects the morphology, solubility, lattice parameters and consequently the stability of the material [10]. The incorporation of cations other than Ca^{2+} generally induces a decrease in the structure stability [11 and references herein reported]: the destabilizing effect of some ions such as Mg^{2+}, Mn^{2+}, Fe^{2+}, Co^{2+} and Ni^{2+} is so evident that they inhibit the synthesis of HA promoting the formation of β-tricalcium phosphate (β-TCP). In fact, even at low concentration, they severely strain the HA structure up to its collapse [11] due to the large difference in ionic radii [12] that makes impossible the formation of the metal to oxygen bonds. This is a consequence of the atomic arrangement; in fact the ten Ca^{2+} ions in the unit cell exist in two polyhedra (Ca1 and Ca2). Ca1 coordinates to nine oxygen ions, six of which (3 O1 and 3 O2) in planes ½ unit cell above and below the central cation form a trigonal prism; three more oxygen atoms (3 O3) essentially coplanar with Ca1 are bonded through the prism face to form three capped trigonal prisms. Ca2 bonds to six oxygen atoms (O1, O2 and 4 O3) and one OH^- group [1]. Loss of apatite structural integrity is probably preceded by phase transformation from $P6_3/m$ to a range of polymorphs-hexagonal, monoclinic, triclinic ($P6_3$, P-3, P-6, $P2_1/m$ and $P2_1$) due to framework distortion and cation ordering [13]. It must be emphasized that in natural apatite the solubility limit for the above cited cations is generally lower than 15 mol% [1]. Therefore, it is necessary to understand the relationships between chemical and structural aspects and the material properties to obtain doped monophasic compounds.

Recent literature suggests that Fe^{3+} could get in the apatite structure [14]; the amount of Fe^{3+} substituting for Ca in the HA structure is temperature dependent and varies from 0.5 after annealing at 600 °C to 0.2 at 1000 °C [15]. According to Mössbauer spectroscopy, the dissolution of iron(III) into the apatite structure is very complex and the phases that are formed depend on the synthesis method, on the Fe/P and Fe/Ca ratios, and, in the case of the ceramic synthesis, on the thermal treatment [15]. This complexity is obviously connected with the low solubility of iron in hydroxyapatite due to the differences in the ionic radii between Ca^{2+} and Fe^{3+} and, most importantly, in the charges, that give rise either to the formation of a non stoichiometric compound or to other possible charge compensation mechanisms. On the other side, [16] in the paper dealing with Fe^{2+} incorporation in hydroxyapatite were not able to provide definitive answers about the iron solubility limits and its distribution between Ca1 and Ca2. Mössbauer spectroscopy studies suggest that Fe^{2+} is randomly distributed between the Ca1 and Ca2 sites in Fe-diluted (<1% mol) fluorapatite, but has a strong preference for Ca1 at concentrations approaching the solubility limits [17].

The research work presented here had started out with the goal of reproducing the preparative work described in [18] and, once the single phase hydroxyapatite was obtained, to synthesize Fe^{3+}-doped hydroxyapatite samples, substituting the Ca^{2+} ions with the Fe^{3+} ions, to study the structural variations and the Mössbauer properties of the samples upon the increase of Fe^{3+} concentration. We used two different preparation methods for synthesizing the calcium hydroxyapatite undoped and doped with iron: the ceramic and the hydrothermal methods. The former is a high temperature method, involving chemical reactions by ionic diffusion, starting from solid substances such as oxides or carbonates. The hydrothermal method is completely different from the ceramic one. In fact, in this case a solution containing all the precursors is initially prepared and put into a pressure reactor. Then, the precipitation of the iron-doped hydroxyapatite is induced by the pressure generated by the solvent inside the reactor when heated at relatively low temperatures, typically of 150–200 °C. We found it interesting to explore different methods in order to highlight the best method to prepare single phase calcium hydroxyapatite. Moreover, the aim was also to investigate the role of the dopant element within the synthesis method. As the results were quite unexpected and not in close agreement with what reported in the literature, the research work received new goals:

- to evaluate the role of the precursors of calcium and phosphorus utilized for the synthesis of undoped- or Fe^{3+}-doped hydroxyapatites, prepared by ceramic and hydrothermal synthesis;
- to evaluate the roles of the various preparative procedures and of the thermal treatment in the obtainment of monophasic systems.

Experimental

Chemicals

Chemicals were purchased at the highest commercially available purity and used without further treatment. Calcium carbonate (99.5%) and sodium dihydrogen phosphate ($(NH_4)H_2PO_4$) (98.0%) were obtained from Carlo Erba; calcium oxide (96.0) from Riedel; phosphoric acid (H_3PO_4) (85.0%) from Eurobase; iron(III) oxide (99.9%) from

Aldrich; iron(III) nitrate (98.0%) and ammonium hydroxide (water solution 28%) from Baker; citric acid (99.5%) from Fluka and sodium dodecyl sulphate (90.0%) from Merck.

Synthesis methods

Ceramic synthesis

The synthesis method followed for the preparation of all the samples reported in Table 1 is almost constant in all the cases and the details are shown in the same table; so only a brief summary is here reported.

The procedure consists in the mixing of appropriate quantities of powders of the calcium and phosphate precursors in a molar ratio Ca:P = 1.67:1. The mixture so obtained was thoroughly mixed in an agate mortar and pelletized. The pellets were heat treated, ground and pelletized again and an eventual second heat treatment was performed. The precursors utilized were $CaCO_3$ and CaO for Calcium and $(NH_4)H_2PO_4$ for phosphorus, and are reported in Table 1.

The theoretical mass balances for the calcium hydroxyapatite, starting from the calcium and phosphorous precursors, can be written as follows:

$$10CaCO_3 + 6(NH_4)H_2PO_4 \rightarrow Ca_{10}(PO_4)_6(OH)_2 + 10CO_2 + 8H_2O + 6NH_3 \quad (1)$$

$$10CaO + 6(NH_4)H_2PO_4 \rightarrow Ca_{10}(PO_4)_6(OH)_2 + 8H_2O + 6NH_3 \quad (2)$$

The doped samples have been prepared according to the same procedure as the pure ones, but utilizing Fe_2O_3 and $Fe(NO_3)_3$ as iron precursors. This implied the decreasing of the Ca precursor amount so that the ratio (Ca + Fe):P = 1.67:1 was respected. The details of the syntheses are reported in Table 1 where the samples are indicated with the letter C for the ceramic synthesis, preceded, when necessary, by the nominal Fe percentage and followed by a number referring to thermal treatment as illustrated in Table 1.

Hydrothermal synthesis

A general synthesis method is shortly reported in the following whilst the details are presented in Table 2. Appropriate amounts of CaO, H_3PO_4 and of a surfactant (sodium dodecyl sulphate, SDS) or a complexing agent (citric acid) were dissolved in water and the pH fixed at the values reported in Table 2 by addition of NH_4OH. The obtained colloidal suspension was placed in an autoclave and heated at 240 °C for 96 h. Afterwards the suspension was cooled at room temperature and filtered. The obtained white solid was washed with water and dried at 90 °C for 2 h. Different iron precursors were used for the doped

Table 1 Ca, P and Fe precursors used for the ceramic syntheses and thermal treatments

Sample	Ca^{2+}	$(PO_4)^{3-}$	Fe^{3+}	Highest temp (°C)	Time (h)	Highest temp (°C)	Time (h)	Highest temp (°C)	Time (h)
C1	$CaCO_3$	$(NH_4)H_2PO_4$	–	800	2	–	–	–	–
C2	$CaCO_3$	$(NH_4)H_2PO_4$	–	800	2	800	2	–	–
C3	$CaCO_3$	$(NH_4)_2HPO_4$	–	950	2	1100	48	–	–
C4	CaO/H_2O	$(NH_4)H_2PO_4$	–	800	4	–	–	–	–
Fe0.1C2	$CaCO_3$	$(NH_4)H_2PO_4$	Fe_2O_3	800	2	800	2	–	–
Fe0.5C2	$CaCO_3$	$(NH_4)H_2PO_4$	Fe_2O_3	800	2	800	2	–	–
Fe1.0C2	$CaCO_3$	$(NH_4)H_2PO_4$	Fe_2O_3	800	2	800	2	–	–
Fe5.0C2	$CaCO_3$	$(NH_4)H_2PO_4$	Fe_2O_3	800	2	800	2	–	–
Fe0.1C5	$CaCO_3$	$(NH_4)H_2PO_4$	Fe_2O_3	800	2	800	2	900	15
Fe0.5C5	$CaCO_3$	$(NH_4)H_2PO_4$	Fe_2O_3	800	2	800	2	900	15
Fe1.0C5	$CaCO_3$	$(NH_4)H_2PO_4$	Fe_2O_3	800	2	800	2	900	15
Fe5.0C5	$CaCO_3$	$(NH_4)H_2PO_4$	Fe_2O_3	800	2	800	2	900	15
Fe5.0C1	$CaCO_3$	$(NH_4)H_2PO_4$	$Fe(NO_3)_3$	800	2	–	–	–	–
Fe0.5C6	$CaCO_3$	$(NH_4)_2HPO_4$	Fe_2O_3	950	2	1100	48	1200	24
Fe1.0C6	$CaCO_3$	$(NH_4)_2HPO_4$	Fe_2O_3	950	2	1100	48	1200	24
Fe5.0C6	$CaCO_3$	$(NH_4)_2HPO_4$	Fe_2O_3	950	2	1100	48	1200	24
Fe10C7	$CaCO_3$	$(NH_4)_2HPO_4$	Fe_2O_3	950	2	1100	48	1200	72
Fe15C8	$CaCO_3$	$(NH_4)_2HPO_4$	Fe_2O_3	950	2	1100	48	1450	48

Table 2 Preparation conditions for the hydrothermal synthesis: Fe precursors, complexing agents, pH values

Sample	Ca^{2+}	$(PO_4)^{3-}$	Complexing agent	Fe^{3+}/Fe^{2+}	pH solution	Highest temp (°C)	Time (h)
H8	CaO	H_3PO_4	–	–	8	240	96
H10	CaO	H_3PO_4	–	–	10	240	96
H11	CaO	H_3PO_4	–	–	11.10	240	96
H10S	CaO	H_3PO_4	SDS	–	10	240	96
H10C	CaO	H_3PO_4	Citric acid	–	10	240	96
Fe3HC	CaO	H_3PO_4	Citric acid	$Fe(NO_3)_3$	10	240	96
Fe3HC500	CaO	H_3PO_4	Citric acid	$Fe(NO_3)_3$	10	240	96
Fe2HC	CaO	H_3PO_4	Citric acid	$Fe(CH_3COO)_2$	10	240	96
Fe2HC500	CaO	H_3PO_4	Citric acid	$Fe(CH_3COO)_2$	10	240	96

samples. When the iron(II) precursor was used, all the operations were carried out under nitrogen and using deoxygenated water. Part of each doped sample was then heated in the air at 500 °C for 1 h (Samples Fe3HC500 and Fe2HC500, respectively). Detailed experimental conditions are reported in Table 2 where the samples are indicated with the letter H for hydrothermal synthesis followed by a number indicating the pH and, when necessary a letter for the complexing agent. For the doped samples letter H is preceded by the nominal Fe percentage and eventually followed by the temperature of thermal treatment.

Characterization techniques

X-ray powder diffraction

X-ray powder diffraction (XRPD) data were collected on a computer-controlled Philips X'Pert Pro diffractometer. A vertical goniometer, using conventional Bragg–Brentano parafocussing geometry, was equipped with incident and diffracted beam Soller slits, with fixed 1° and 0.1 mm divergence and receiving slits, respectively, curved graphite diffracted beam monochromator and scintillation counter. The long fine-focus Cu X-ray tube operated at 40 kV and 40 mA. Data were recorded in the 3°–70° 2θ range, in continuous-scan mode with step width increments of 0.02° and a step counting time of 0.5 s. Collected data were processed by X'Pert Software (Philips copyright) [19]. Semi-quantitative analyses were performed using X'Pert High Score software (Philips copyright) [19] to determine the mass fraction on the basis of the RIR (Reference Intensity Ratio) values taken from the software database. It should be pointed out that the method gives exact results, but we consider the estimates as semi-quantitative estimates because results are in reality affected by several errors. The main one is that RIR values from the reference database are inaccurate. However, in this study the same RIR values are used and therefore self-consistent results are obtained.

Mössbauer spectroscopy

Mössbauer spectra were recorded on a conventional constant-acceleration spectrometer, which used a room temperature Rh matrix ^{57}Co source. Spectra were collected at RT and at 10 K using a closed-circuit cryostat, but only the data at RT are reported as no relevant information, other than the absence of any superparamagnetic material, were obtained from the 10 K spectra. The hyperfine parameters isomer shift (δ), quadrupole splitting (ΔE_Q) or shift (ε), full line width at half maximum (Γ), all expressed in mm/s, and internal magnetic field (B), expressed in Tesla, were obtained by a standard least-squares minimisation technique and are reported in Tables 5 and 6. The spectra were fitted to Lorentzian line shapes using the minimum number of sextets and doublets. Isomer shift is quoted relative to metallic iron at room temperature.

Infrared spectroscopy

Room temperature absorption spectra in the medium infrared region (400–4000 cm^{-1}) were measured with a Magna 740 FTIR spectrometer. The spectral resolution of the absorption spectra was 2 cm^{-1}. The sample was thoroughly mixed with anhydrous KBr (about 1% in mass of the sample with respect to the KBr) and pelletized with a hydraulic press at 10 tons.

Results and discussion

X-ray diffraction

X-ray diffraction patterns (Fig. 1) of all the samples show sharp and narrow peaks attributable to apatite (HA) and to other phases (Tables 3, 4).

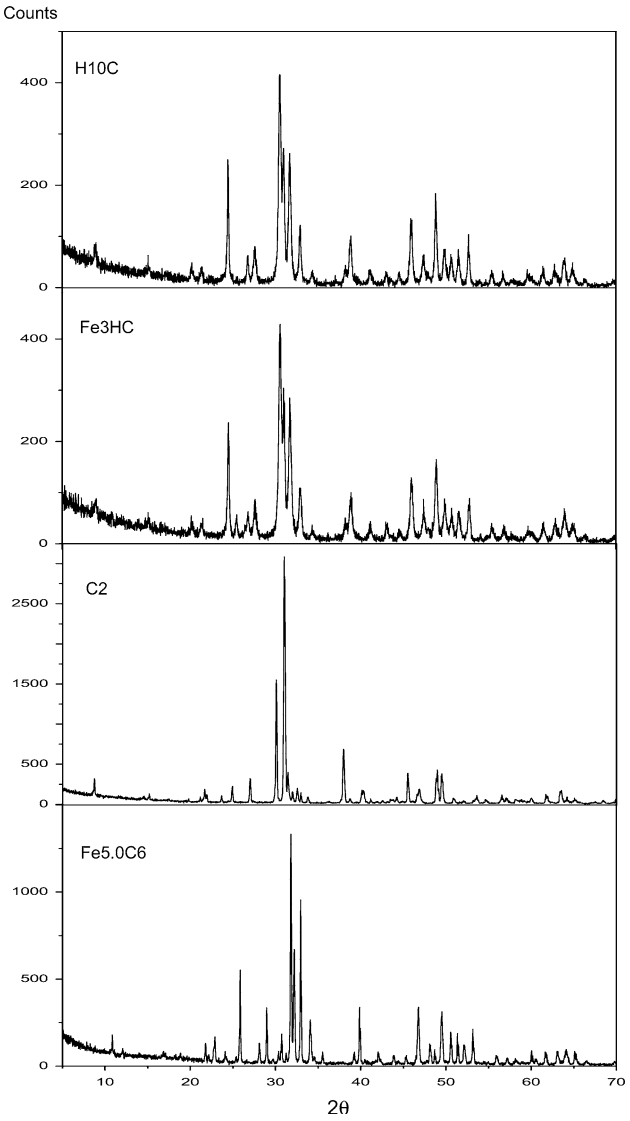

Fig. 1 X-ray powder diffraction of some samples prepared by ceramic and hydrothermal synthesis

Table 4 Crystalline phases and their semi-quantitative percentages for Fe^{3+}-doped samples, as estimated by XRPD data

Sample	HA	$Ca_3(PO_4)_2$	Fe_2O_3	Fe-phos
Fe0.5C6	100	0	0	–
Fe1.0C6	69	31	0	–
Fe5.0C6	39	61	0	–
Fe10C7	0	96	4	–
Fe15C8	0	96	4	–
Fe3HC	90	–	–	10
Fe3HC500	90	–	–	10
Fe2HC	90	–	–	10
Fe2HC500	90	–	–	10

Fe-phos is a non-identified Fe phosphate because the few peaks present in the diffractogram are compatible with various species

Ceramic synthesis

Samples C1, C2 and C4, prepared by using different reagents, allow one to evaluate the role of the various Ca and P precursors used in the syntheses by the ceramic method because comparable thermal treatments have been used in all the procedures (Table 1).

Samples C1 and C2, prepared by using $CaCO_3$ as the Ca precursor, are polyphasic mixtures, each with a different component distribution, containing hydroxyapatite (41 and 28%, respectively, Fig. 2), $Ca(PO_3)_2$, $Ca_2P_2O_7$ and $Ca_3(PO_4)_2$ (Table 3); variable, but small amounts of CaO, $CaCO_3$ and $Ca(OH)_2$ are also present (Table 3) in C1. The second heating step (sample C2) causes the complete decomposition of the carbonate whose peaks are no longer evident in the XRP diffractogram. It is not easy to rationalize the coexistence of the various phosphatic phases in these two samples. According to the literature [20, 21], an amorphous $Ca(PO_3)_2$ is formed at a temperature as low as 250 °C; it crystallizes at 500 °C, transforms into $Ca_2P_2O_7$

Table 3 Crystalline phases and their semi-quantitative percentages for undoped samples, as estimated by XRPD data

Sample	HA	CaO	$Ca(OH)_2$	$CaCO_3$	$Ca(PO_3)_2$	$Ca_2P_2O_7$	$Ca_3(PO_4)_2$	$CaHPO_4$
C1	41	2	4	6	15	15	16	–
C2	28	9	1	–	10	29	23	–
C3	90	10	–	–	–	–	–	–
C4	–	–	–	–	–	77	23	–
H8	60	–	–	–	–	–	–	40
H10	84	–	–	–	–	–	16	–
H11	82	–	–	–	–	–	18	–
H10S	100	–	–	–	–	–	–	–
H10C	100	–	–	–	–	–	–	–

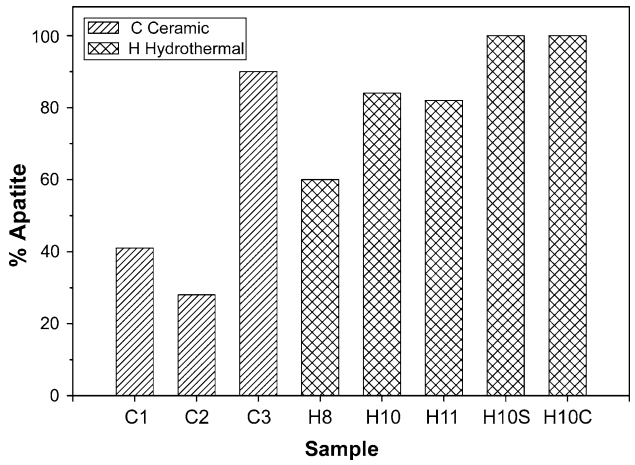

Fig. 2 Percentage of calcium apatite obtained following the different procedure for ceramic and hydrothermal reactions, as estimated by XRPD

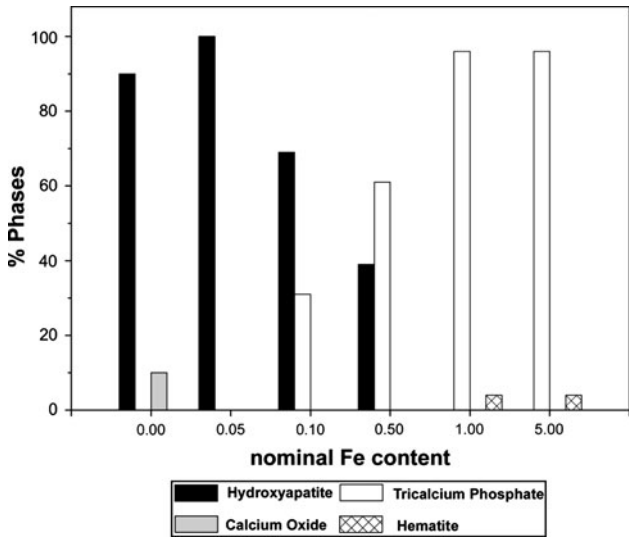

Fig. 3 Percentage of crystalline phases obtained for high temperature-doped samples as a function of the nominal iron content, as estimated by XRPD

between 600 and 750 °C and finally at a higher temperature into $Ca_3(PO_4)_2$. This last compound can also be produced by direct hydroxyapatite decomposition at a temperature higher than 800 °C [22]. This is confirmed by sample C3, synthesized at a higher temperature, 950 °C and then heated to 1100 °C (Table 1), which shows the presence of hydroxyapatite and Calcium oxide in agreement with the $CaO–P_2O_5–H_2O$ phase diagram [23]. The results point out that, in contradiction with the literature, at a temperature of 800 °C and with the chosen thermal treatment, the role of the calcium precursor is fundamental for the crystallization of hydroxyapatite.

The study of the iron-doped compounds does not lead to relevant differences in the phase composition respect to the undoped ones, when prepared according to the same procedure. In particular the XRPD pattern of the samples belonging to the FeXC2 series, analogous to the undoped C2 sample, show the presence of the same phosphates and in the same relative amounts as for the undoped sample, proving that the dopant does not affect the results of the synthesis in a significant way.

The comparison of the results of the undoped samples with the doped ones, referring to series FeXC2 and FeXC5, the latter thermally treated at 900 °C for 15 h, suggests that the obtainment of polyphasic systems is connected with the thermodynamic stability rather than with the kinetic reaction. Only in the sample nominally doped with 5% iron the presence of haematite was detected, even though Mössbauer spectroscopy results show its presence also at lower Fe nominal concentrations, as discussed in "Mössbauer spectroscopy" section.

The samples synthesized at $T \geq 950$ °C show the presence of hydroxyapatite and/or tricalcium phosphate (TCP) phases, the relative amounts depending on nominal composition and/or thermal treatment (Table 4; Fig. 3). The data indicate that hydroxyapatite decreases from 100 to 39% for Fe varying from 0.5 to 5% with the same thermal treatment ($T = 1200$ °C and $t = 24$ h), with the simultaneous TCP increases from 0 to 61%. A higher nominal iron content (10 and 15%) and a longer treatment at the same temperature ($t = 72$ h and $T = 1200$ °C, sample Fe10C7) or a longer treatment at a higher temperature ($T = 1450$° and $t = 48$ h, sample Fe15C8) induce the disappearance of hydroxyapatite in agreement with the results obtained by Kannan et al. [24]. The samples are in fact constituted by tricalcium phosphate and haematite, in agreement with Mössbauer results as discussed in "Mössbauer spectroscopy" section.

Hydrothermal synthesis

The results obtained on the samples prepared by the hydrothermal synthesis show that these materials are richer in the HA phase than samples prepared by ceramic synthesis. All the syntheses (Table 3) produced a large percentage of hydroxyapatite, that becomes the only phase present at pH = 10 in the presence of SDS or citric acid (samples H10S and H10C, respectively; Table 3). The use of the surfactant at pH = 10 is considered particularly efficient in obtaining a monophasic system [25], sample H10S. The role of the surfactant may be explained by considering its behaviour in solution and its electronic and structural properties. In aqueous solution SDS is completely ionized producing a sulphonate group with a tetrahedral structure very similar to that of the phosphate group. In an aqueous solution of SDS and phosphate ions, micelles containing numerous phosphate groups on the

surface are probably produced and they can thus be considered as the nucleation point for the growth of hydroxyapatite crystals [25, 26].

The synthesis in the presence of citrate leads to an analogous result (H10C) by the formation of an anionic adduct according to the reaction $Ca^{2+} + (C_6H_8O_6)^{3-} \rightarrow [Ca(C_6H_8O_6)]^-$ avoiding the precipitation of $Ca(OH)_2$. On increasing the temperature the dissociation constant of the complex increases, so that Ca^{2+} is released in the presence of the phosphate group and the hydroxyapatite can be formed and precipitated.

As far as the other samples prepared by the hydrothermal procedure are concerned, the presence of a small amount of $Ca_3(PO_4)_2$ in samples H10 and H11 is not surprising, whilst it is much more difficult to explain the coexistence of hydroxyapatite and $CaHPO_4$ in the sample H8. In this case, the results can be explained considering that at 240 °C and at pH = 8 the concentration of HPO_4^{2-} may be higher than that of PO_4^{3-} or that the solubility of $CaHPO_4$ becomes lower than that of $Ca_3(PO_4)_2$ [27]. The iron-doped samples are constituted by a biphasic system composed by hydroxyapatite (90%) and an iron phosphate (10%) (Table 4), whose identification is not simple because just one diffraction peak did not overlap with the hydroxyapatite ones in the XRPD pattern.

Infrared spectroscopy

Ceramic synthesis

The infrared absorption spectra of the various samples prepared by both the ceramic and the hydrothermal procedures were measured at room temperature. It is worth mentioning that in the unit cell of the calcium hydroxyapatite 44 atoms are present, giving rise to 132 vibrational modes. From a factor group analysis, it was found that 42 infrared-active modes are possible, amongst which 18 are internal modes involving the phosphate groups. According to a site group analysis, these internal modes can be subdivided into the v_i (i = 1–4) modes of the PO_4 tetrahedron. The spectrum of the C1 sample shows the characteristic absorptions of the phosphate and of the hydroxide groups, in agreement with that reported in the literature by Fowler [28] for a calcium hydroxyapatite sample (Fig. 4). The features observed around 600 cm^{-1} are attributed to bending v_4 modes, whilst the bands around 1050 cm^{-1} are attributed to symmetric v_1 and asymmetric v_3 stretching modes. The weak band observed at about 450 cm^{-1} can be attributed to the bending v_2 modes. The broad band extending from 3200 to 3600 cm^{-1} indicates the presence of water absorbed in the sample. The narrow band peaking at 3570 cm^{-1} is characteristic of the OH stretching vibration of hydroxyapatite [28]. Absorption bands at 1460, 1419 and 875 cm^{-1} are

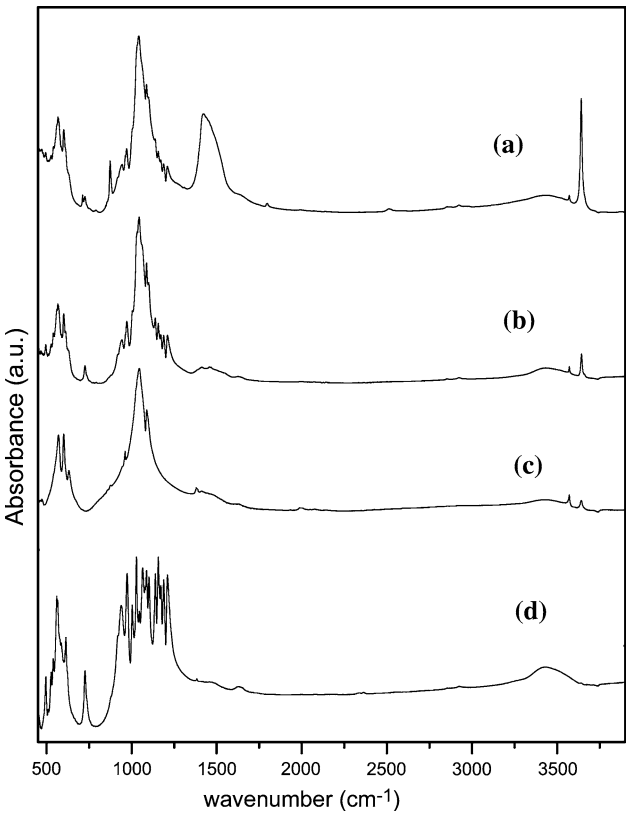

Fig. 4 Infrared FTIR absorption spectra for undoped samples prepared by ceramic synthesis (*a*) C1, (*b*) C2, (*c*) C3, (*d*) C4

assigned to the carbonate ions (CO_3^{2-}), indicating the presence of a carbonate-apatite, in which the carbonate ions occupy the B-site. The carbonate ion in the apatite structure most probably derives from the calcium carbonate used as a starting reagent. Moreover, the absorptions at 713 and 3644 cm^{-1} can be assigned to unreacted $CaCO_3$ [29] and calcium hydroxide [30], respectively. Some overlapping bands, in the 700–1200 cm^{-1} region, are observed, which are assigned to pyrophosphate ions [31, 32], in agreement with X-ray results (Table 3). The infrared spectrum of the C2 sample is similar to that of C1, but some differences can be observed. First, the band at 713 cm^{-1} is absent, indicating the complete decomposition of calcium carbonate with the second heat treatment. The bands attributed to the carbonate ions in the apatite structure almost disappear, suggesting a release of CO_2 on increasing the annealing time. This behaviour is in agreement with X-ray results (Table 3). The reduction of the amount of calcium hydroxide is also confirmed by the decrease of the intensity of the band at 3644 cm^{-1}. Bands due to the pyrophosphate ions are present, confirming the presence of $Ca_2P_2O_7$, which is also the most abundant phase from X-ray results. The absorption spectrum of the C4 sample (Fig. 4) is dominated by bands due to calcium pyrophosphate and also TCP, which strongly overlap.

The comparison between the absorption bands for an undoped sample (not shown) and iron-doped samples prepared using the procedure indicated as FeXC2 (Table 1) shows that the doped samples contain the usual phases found in the undoped ones (see XRPD data, Table 3). Nonetheless, the amount of carbonate-apatite and unreacted calcium carbonate phases are higher for the iron-doped samples, indicating a minor extent of the solid state reaction. Due to the low iron nominal concentration, it is not possible to clearly identify the iron oxide phase using IR spectroscopy (Table 3). Moreover, the preparation procedure indicated as FeXC5 does not lead to different results, indicating that a further treatment at 900 °C is not useful in order to obtain single phase hydroxyapatite.

It is worth noting that for the iron-doped ceramic samples annealed at high temperature the band due to the OH^- group is present for the 0.5% iron-doped sample, whilst it is not observed for the 10% iron-doped one. This behaviour suggests that there are no OH^- groups in the more concentrated iron sample, and this is consistent with the results obtained from the X-ray analysis (Table 3). In fact, from this analysis, it was found that on increasing the iron concentration and the annealing temperature, the percentage of the apatite phase decreases (Table 3). The 0.5% sample is constituted by a hydroxyapatite single phase whilst in the 10% doped sample the hydroxyapatite phase is absent and the only phase present is calcium phosphate.

Hydrothermal synthesis

The infrared spectra for the samples prepared by different hydrothermal syntheses (Fig. 5) are very similar to each other, and they consist of typical bands due to the HA phase [28], in agreement with the XRPD results. On the other hand, the bands due to other phases found in the XRPD analyses (TCP and $CaHPO_4$) are hardly visible in the infrared spectra because of their low percentage amount and the strong overlap with those of the hydroxyapatite phase.

Mössbauer spectroscopy

The spectra of the samples prepared by the ceramic method (Table 5) are rather complex, showing the presence of various paramagnetic and magnetic components; the presence of various phases and of more than one site available to iron in each phase make the interpretation of the spectra in any case difficult and generally not definitive.

Entering into the details, the spectrum of Fe0.5C6 shows the presence of two paramagnetic and two magnetic iron components in a ratio of approximately 1:1. Considering that in the XPRD pattern only hydroxyapatite is evident, the two doublets are imputable to iron occupying the two calcium sites in the phosphate structure (Fig. 6). Site Ca(1)

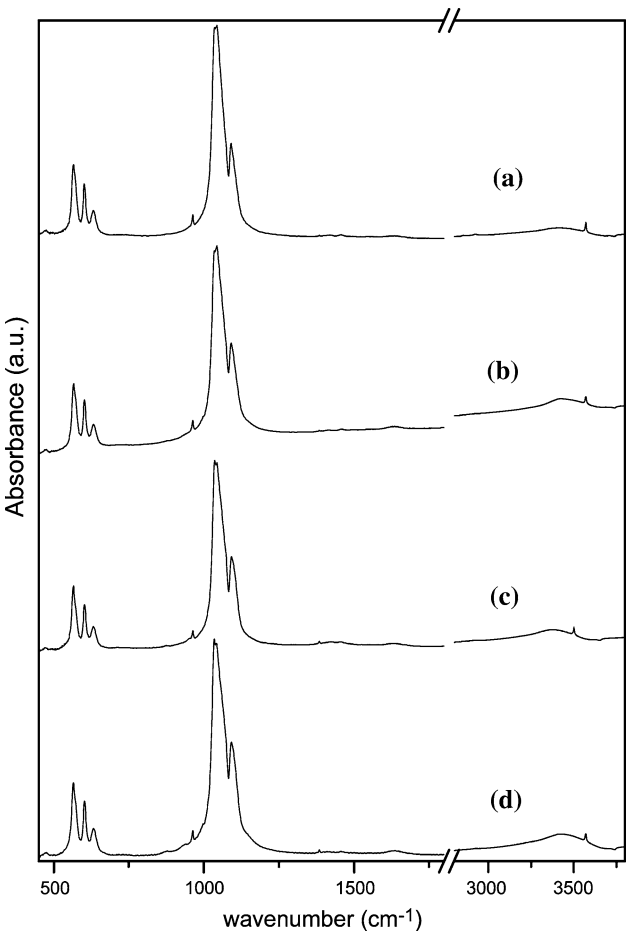

Fig. 5 Infrared FTIR absorption spectra for iron-doped samples prepared by hydrothermal synthesis: (*a*) Fe3HC, (*b*) Fe3HC500, (*c*) Fe2HC, (*d*) Fe2HC500

is a very large cavity in which Ca^{2+} is coordinated with nine oxygen atoms [1]. In this site the iron atom may either be coordinated with the same oxygens as calcium, but thanks to the large dimensions of the site, it can also be accommodated far away from the centre of the cavity so that it is bonded only to the four closest oxygens. Site Ca(2) bonds to six oxygen atoms and one column anion (OH^-, Cl^-) in which the iron atom can easily be hosted. According to theoretical calculations, the most stable geometry for iron(III) seems to be the Ca(1) site, followed by Ca(2) [12]. Consequently, Fe1 in Table 5, with the lowest isomer shift value, is thought to occupy the Ca(1) site and Fe2, with the highest isomer shift, the Ca(2) site [12]. The different quadrupole splitting values may be due to the fact that whilst Fe1 is coordinated with only phosphate oxygens, Fe2 is bonded also to a hydroxide oxygen, creating an asymmetry in the electron density around the iron centre that gives rise to a strong contribution to the quadrupole splitting. The two magnetic components, not attributable to species detected in the XRPD pattern

Table 5 Mössbauer effect parameters at RT for the samples prepared by the ceramic synthesis

Sample	Site	δ (mm/s)	ΔE_Q or ε (mm/s)	B (T)	Γ (mm/s)	A (%)	Attribution
^{57}Fe0.5C6	Fe1	0.07	1.03	–	0.27	13	Ca(1) HA
	Fe2	0.24	1.55	–	0.46	40	Ca(2) HA
	M1	0.34	−0.53	50.8	0.37	25	Ferrite ($Ca_2Fe_2O_5$)
	M2	0.17	0.69	43.4	0.31	22	Ferrite ($Ca_2Fe_2O_5$)
Fe1.0C6	Fe1	0.14	1.05	–	0.43	58	Ca(1) HA
	Fe2	0.34	1.42	–	0.41	38	Ca(2) HA
	Fe3	0.47	2.11	–	0.22	4	TCP
Fe5.0C6	Fe1	0.17	1.10	–	0.43	44	HA
	Fe2	0.26	1.57	–	0.33	38	HA
	Fe3	0.24	1.98	–	0.31	18	TCP
Fe10C7	M1	0.37	−0.10	51.7	0.33	100	Haematite
Fe10C8	Fe(II)	1.13	0.81	–	0.44	24	Fe^{2+} (Ca2)
	M1	0.37	−0.18	51.7	0.27	61+5	Haematite + Magnetite
	M	0.67	0.06	46.1	0.31	9	Magnetite
Fe0.5C2	Fe4	1.08	2.60	–	0.65	8	Fe(II) T (Ca2)
	Fe5	0.42	0.56	–	0.72	37	Fe(III) M
	M1	0.37	−0.22	51.3	0.388	55	Haematite
Fe0.5C5	Fe4	1.03	2.53	–	0.70[a]	22	Fe(II) T (Ca2)
	Fe5	0.46	0.50[a]	–	0.64	36	Fe(III) M
	M1	0.37	−0.15	51.9	0.41	42	Haematite
Fe1.0C2	Fe4	1.01[a]	2.57	–	0.70[a]	11	Fe(II) T (Ca2)
	Fe5	0.43	0.50	–	0.52[a]	21	Fe(III) M
	M1	0.37	−0.22	51.4	0.40	59	Haematite + ferrite
	M2	0.21	0.64	43.6	0.57	9	Ferrite ($Ca_2Fe_2O_5$)
Fe1.0C5	Fe4	0.98	2.47	–	2.47	24	Fe(II) T (Ca2)
	Fe5	0.35	0.66	–	0.80	18	Fe(III) M
	M1	0.37	−0.21	51.6	0.43	50	Haematite + ferrite
	M2	0.19	0.70	44.0	0.700	9	Ferrite ($Ca_2Fe_2O_5$)
Fe5.0C2	Fe5	0.40	0.41	–	0.91	30	Fe(III) M
	M1	0.35	−0.22	51.6	0.62	70	Haematite
Fe5.0C1	Fe5	0.38	0.62	–	0.28	6	Fe(III) M
	FeP	0.43	–	–	1.29	65	$Ca_9Fe(PO_4)_7$
	M1	0.37	−0.18	51.9	0.23	29	Haematite

δ data are referred to room temperature α-iron foil

[a] Parameters constrained in the fitting procedure

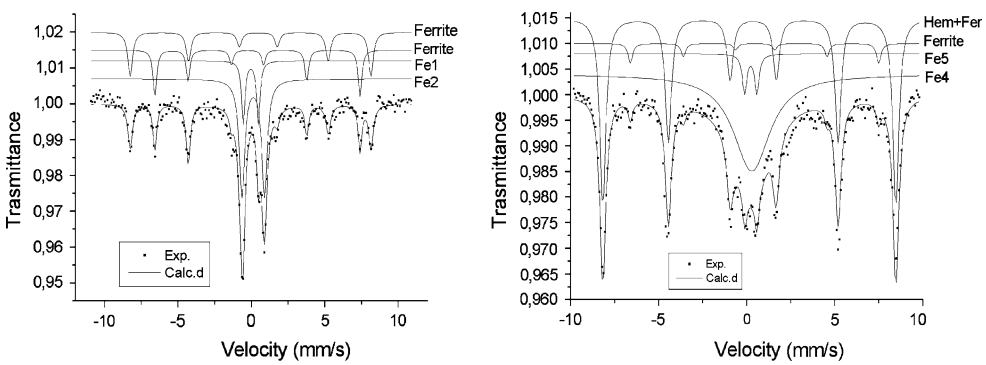

Fig. 6 Mössbauer effect spectra of ^{57}Fe0.5C6 (**a**) and Fe1.0C5 (**b**). **a** *Dashed lines* for subspectra of M1 and M2 ferrite sites, *continuous lines* for subspectra of Fe1 and Fe2 ferric sites. **b** *Dashed lines* for subspectra of M1 and M2 ferrite and haematite sites, *continuous line*s for subspectrum of Fe5 ferric site and dotted line for subspectrum of Fe4 ferrous site

because of their low presence, may be due to calcium ferrite, $Ca_2Fe_2O_5$, which is known to form by reaction of $CaCO_3$ with haematite at 720 °C [33, 34]. This oxide is characterized by two different iron(III) containing sites occupied in a 1:1 ratio, one of which presents octahedral coordination geometry and should be responsible for the largest sextet ($B = 50.9$ T at RT), whilst the other has a tetrahedral coordination geometry and gives rise to the narrowest sextet ($B = 43.3$ T at RT).

On increasing the iron content, the situation becomes even more complex and strongly dependent on the thermal treatment. In fact, in the spectrum of sample Fe1.0C6 the magnetic phases completely disappears, the two paramagnetic doublets seem to maintain the same coordination geometry as in Fe0.5C6 and are therefore again attributed to the Ca(1) and Ca(2) sites in the apatite structure, and a new iron species appears. This gives rise to a third very weak doublet with an isomer shift of 0.47 mm/s; such absorption has been attributed either to a very asymmetric iron(III) site in the TCP structure on the basis of the XRPD or to amorphous iron(III) [15]. With a further increase of the iron content, sample Fe5.0C6, the dissolution of iron(III) in TCP increases as evident from the Mössbauer spectrum that now shows the presence of three different iron centres, two reasonably imputable to HA and the third one to TCP (Fe3). This last coordination site is very distorted, as proved by the very high quadrupole splitting value, 1.98 mm/s at RT, and this fact may justify the difficulty with which iron enters the phosphate lattice; in fact when iron content was only 1%, TCP was already present in the mixture, but without any trace of iron. A higher iron content (10%) and a longer heat treatment, sample Fe10C7, cause the expulsion of all iron ions from the phosphatic phases and only macrocrystalline haematite is now evident in the RT Mössbauer spectrum, a phase also detected in the XRPD pattern. The reasons for this unexpected behaviour are not easy to understand, but it may be supposed that small and uncontrollable variations in the synthesis procedure, such as slightly different grinding or homogeneity of the pallet can lead to completely different results. The Mössbauer spectrum of the highest doped sample, Fe15C8, heated to the highest temperature and for the longest time is quite different from the previous ones. In fact at RT the paramagnetic part is completely due to an octahedral iron(II) species whilst the magnetic component is now formed, besides haematite, also by magnetite. The presence of magnetite is evident thanks to the sextet due to the tetrahedral $Fe^{2.5+}$ species that is not hidden by the haematite one; considering the intensity of this sextet, it was possible to subtract the magnetite contribution to the high field sextet and attribute all the remaining absorption to haematite. The iron reduction at high temperature in the presence of oxygen is a known reaction already reported for iron phosphate glasses [35] and is made possible by the increase of the entropy of the system due to the formation of gaseous oxygen. It is probably the formation of iron(II) cations with dimensions fitting the Ca(2) coordination site, besides the identity of the formal charge between iron and calcium, that makes possible the formation of phosphate phases that were not stable with 10% iron(III).

The samples of the series FeXC2 and FeXC5 (Table 5) were heated for shorter times and at lower temperatures compared to those of the series FeXC6, FeXC7 and FeXC8, and the resulting spectra are, surprisingly, rather different, the main differences being the constant presence of haematite and, in the samples with a nominal iron content of up to 1%, of tetrahedral iron(II). These results seem to stress the importance of the kinetic aspects in the evolution of the system. In fact haematite seems to form at the early stages of the reaction, dissolving later in the phosphate phases. In a similar way iron(III) is first reduced to balance the different charges between Ca^{2+} and Fe^{3+} and guarantee the electronic neutrality of the phosphate and then re-oxidized by the oxygen present in the furnace atmosphere giving rise to different phosphate structures. This is proved by the fact that the parameters of the iron sites in the two series never match. The only constant presence in the two series is that of ferrite, one of whose sextets overlaps the haematite one. As in the previous series, this component disappears at the highest nominal iron content (5%). On the basis of the ΔE_Q values [18] Fe4 is believed to occupy the Ca(I) site with a tetrahedral coordination geometry. In the sample with the highest iron concentration a very broad singlet becomes evident, with parameters that are not greatly influenced by the temperature and that has been attributed to $Ca_9Fe(PO_4)_7$ [36] in agreement with the XRPD results.

The most relevant feature of the Mössbauer spectra of the samples prepared by hydrothermal synthesis (Table 6) is the absence of any magnetic component even at low temperature. This means that citric acid was able to complex both iron(II) and iron(III), avoiding the formation of hydroxide species at least in the reaction conditions, allowing the entrance of the cations into the phosphate lattices. Several paramagnetic doublets are consequently present in each spectrum making the attributions quite difficult and not definitive. As the iron-doped samples are constituted only by hydroxyapatite (90%) and an iron phosphate (10%) (Table 4), comparing the Mössbauer spectrum of this sample with that of Fe0.5C6, formed only by HA, it is possible to assume that all the iron entered the phosphate lattice, evidently more accessible in these experimental conditions, and not in the hydroxyapatite lattice. The only interesting aspect is the appearance of iron(II) species in the sample Fe3HC prepared starting from iron(III) nitrate. The iron reduction is compatible with

Table 6 Mössbauer effect parameters at RT for the samples prepared by the hydrothermal synthesis

Sample	δ (mm/s)	ΔE_Q (mm/s)	Γ (mm/s)	A (%)	Attribution
Fe3HC	1.21	2.26	0.65	26	Fe(II) M
	1.08	3.46	0.24	7	Fe(II) Ca(1) HA
	0.36	0.63	0.98	39	Fe(III) M
	0.41	0.39	0.26	27	Fe(III) M
Fe2HC	1.20	2.26[a]	0.68	43	Fe(II) M
	1.12	0.98[a]	0.40	11	Fe(II) Ca(2) HA
	0.42	0.79	0.49	46	Fe(III) M
Fe3HC500	0.40	0.73	0.41	49	Fe(III) M
	0.42	1.14[a]	0.38	31	Fe(III) M HA
	0.32	1.72[a]	0.59	19	Fe(III) M HA
Fe2HC500	0.39	0.71	0.48	46	Fe(III) M
	0.39	1.14[a]	0.38	10	Fe(III) M HA
	0.34	1.72[a]	0.63	44	Fe(III) M HA

δ data are referred to room temperature α-iron foil

[a] Parameters constrained in the fitting procedure

the presence of iron in the phosphate as a substitute for Ca^{2+}. The iron reduction is a way, often found in similar situations, to compensate for the charge difference between the two cations and to recreate the electric neutrality. Also relevant is the second iron(II) site in the spectrum of Fe3HC whose parameters ($\delta = 1.08$ mm/s, $\Delta E_Q = 3.46$) are in agreement with those reported in the literature [37] for iron(II) occupying the hydroxyapatite Ca(1) site. The thermal treatment of the two samples (500 °C, 1 h) is enough to completely oxidize iron(II) to iron(III) giving rise to nearly identical spectra.

Cell edges

The variation range of a cell edge for the undoped samples is particularly large whilst the values for the c edge remain virtually constant for all the samples (see Table 7). The largest and the smallest values are found for samples C1, C2 and C3 ($a = 9.436(1)$, 9.435(1) and 9.4120(1) Å, respectively; Table 7). Sample C3, prepared at the highest temperature (T = 1100 °C), shows an a cell edge consistent with that of stoichiometric hydroxyapatite ($a = 9.4166$ Å; PDF-file 84-1998). The a cell edge values for C1 and C2 samples are in agreement with the literature ($a = 9.437$ Å; [38] and PDF-file 86-0740) for a type B carbonate-apatite, the presence of which has been evidenced by the analysis of the IR spectra (see "Ceramic synthesis" section). The larger values of a cell edge is due to the twisting Ca(1) trigonal prism in order to favour the substitutions of PO_4 tetrahedra by smaller CO_3 triangles [13, 38]. However, the substitutions of OH- with vacancies in the channel [38] cannot be ruled out.

The samples obtained by the hydrothermal procedure show values practically constant (mean value = 9.4219 Å;

Table 7 Cell dimension data of the HA phases as obtained from X-ray powder patterns

Sample	a (Å)	c (Å)
C1	9.436 (1)	6.882 (1)
C2	9.435 (1)	6.882 (1)
C3	9.4120 (1)	6.8790 (1)
C4	HA not detected	
H8	9.4219 (1)	6.8780 (1)
H10	9.4218 (1)	6.8770 (1)
H11	9.4220 (1)	6.8750 (1)
H10S	9.4217 (1)	6.8850 (1)
H10C	9.4220 (1)	6.8770 (1)
References		
86-0740	9.4350	6.8820
74-0565	9.4240	6.8790
84-1998	9.4117	6.8745
Fe0.1C2	9.399 (1)	6.867 (1)
Fe0.5C2	HA not detected	
Fe1.0C2	9.416 (1)	6.889 (1)
Fe5.0C2	9.431 (1)	6.878 (1)
Fe0.1C5	9.419 (1)	6.882 (1)
Fe0.1C5	HA not detected	
Fe1.0C5	9.432 (1)	6.884 (1)
Fe5.0C5	9.429 (1)	6.879 (1)
Fe5.0C1	HA not detected	
Fe0.5C6	9.408 (1)	6.878 (1)
Fe1.0C6	9.402 (1)	6.876 (1)
Fe1.0C6	9.403 (1)	6.879 (1)
Fe10C7	HA not detected	
Fe15C8	HA not detected	
Fe3HC	9.4162 (1)	6.8728 (1)
Fe3HC500	9.4138 (1)	6.8752 (1)
Fe2HC	9.4177 (3)	6.8704 (4)
Fe2HC500	9.4214 (1)	6.8810 (4)

Values in brackets indicate standard deviation

References correspond to reference code in PDF file

Table 7) and coherent with the reference stoichiometric hydroxyapatite ($a = 9.424$ Å, PDF-file 74-0565; Table 7).

The doped samples prepared by solid state reaction with the same precursors show different behaviours according to the heat treatment temperature. In fact, the samples belonging to the FeXC2 and FeXC5 series prepared at $T = 800$ and 900 °C, respectively, show that the a cell edge variation is not related to the nominal iron content, but depends whether B-type carbonate-apatite is formed (Fe5.0C2, Fe1.0C5) or not (Fe1.0C2 and Fe0.1C2) as evidenced by IR spectra (see "Infrared spectroscopy" section). On the contrary, for the samples prepared at $T = 1200$ °C (series FeXC6) the a lattice parameter decreases from 9.408 to 9.402 Å (Table 7) for iron

percentage varying from 0.5 to 1%, whilst it remains virtually unchanged for a concentration of 5%. The shortening in *a* cell edge, relative to undoped HA (9.412 Å; Table 7), suggests that the small Fe^{3+} ion incorporates into the HA structure. The *a*-axis, virtually unchanged for $x = 5\%$, suggests that Fe^{3+} enters into hydroxyapatite crystals in a smaller amount, corresponding to the fact that it now begins to enter also in TCP, as attested by Mössbauer spectroscopy results (see "Mössbauer spectroscopy" section).

Samples prepared by hydrothermal synthesis show that the *a* cell edge values are not sensitive to the nominal Fe content. The *c* cell edge remains constant throughout all the samples, as already mentioned for the undoped series.

Conclusions

In summary, the results indicate that the proposed goals have been, at least partially, achieved. As a general result, the hydrothermal method appears to be better than the ceramic one to obtain single phase calcium hydroxyapatite samples. The obtained data, however, are not easy to rationalize and so further studies, with a different approach, are necessary. In fact the complementary techniques used have shown that the amount of the products obtained in the present investigation largely depends on the details of the synthesis routes and on the iron concentration. The study of the iron-doped compounds does not lead to relevant differences in the phases composition respect to the undoped ones, when prepared according to the same procedure.

In any case, the obtained results about the behaviour of iron in the synthesis of doped calcium hydroxyapatites are not definitive. The information obtained by Mössbauer spectroscopy are clearly interesting, but, in some cases, not easy to rationalize. In fact in the samples containing only apatite the spectra are compatible with a Fe distribution in the two sites Ca(1) e Ca(2) in agreement with the literature. On the contrary, the spectra of the polyphasic samples cannot be interpreted in a unique way, but at least for the samples heat treated at 800 °C the presence of calcium ferrite is evident, and it must be underlined that it had never been detected before as a product of the apatite synthesis. Moreover, the presence in some samples of Fe^{2+}, probably localized in the Ca(1) site, indicates that a reduction process has taken place to guarantee the charge compensation (samples prepared at high temperature and by the hydrothermal procedure) and that in some cases has led to the formation of magnetite. The frequent presence of haematite seems to indicate a very low solubility of iron in the apatite lattice due to the small sizes of the cation.

The results, although not definitive, agree with conclusions reported in [39], an exhaustive article on crystal structure refinements of ferric-hydroxyapatite synthesized *via* coprecipitation. Therefore, we are encouraged to perform further crystallographic investigations on samples prepared with different synthesis method. Moreover, high temperature experiments on the same samples are now in progress.

Acknowledgement The authors would like to thank Ms. Walton, for the revision of the English text.

References

1. Hughes J, Rakovan J (2002) In: Kohn MJ, Rakovan J, Hughes JM (eds) Phosphates, reviews in mineralogy and geochemistry, vol 48. Mineralogical Society of America, Washington, DC, p 1
2. McConnell D (1973) Apatite: its crystal chemistry mineralogy utilization and geologic and biologic occurrences. Springer Verlag, New York
3. Elliot JC (1994) Structure and chemistry of apatites and other calcium orthophosphates. Elsevier, Amsterdam
4. Aizawa M, Terado T, Howell FS, Itatani K (1999) Res Bull 34:1215
5. Mori K, Hara T, Mizugaki T, Ebitani K, Kaneda K (2004) J Am Chem Soc 126:10657
6. Gross KA, Berndt CC (2002) In: Kohn MJ, Rakovan J, Hughes JM (eds) Phosphates, reviews in mineralogy and geochemistry, vol 48. Mineralogical Society of America, Washington, DC, p 631
7. Pratihar SK, Garg M, Mehra S, Bhattacharyya S (2006) J Mater Sci: Mater Med 17:501
8. Qian J, Kang Y, Zhang W, Li Z (2008) J Mater Sci: Mater Med. 19:3373
9. Merry JC, Gibson IR, Best SM, Bonfield W (1998) J Mater Sci: Mater Med 9:779
10. Pan Y, Fleet ME (2002) In: Kohn MJ, Rakovan J, Hughes JM (eds) Phosphates, reviews in mineralogy and geochemistry, vol 48. Mineralogical Society of America, Washington, DC, p 13
11. Bigi A, Falini G, Foresti E, Gazzano M, Ripamonti A, Roveri N (1996) Acta Crystallogr B 52:87
12. Shannon RD (1976) Acta Crystallogr A 32:751
13. White TJ, ZhiLi Dong (2003) Acta Crystallogr B 593:1
14. Wang J, Nonami T, Yubata K (2008) J Mater Sci: Mater Med 19:2663
15. Low HR, Phonthammachai N, Maignan A, Stewart GA, Bastow TJ, Ma LL, White TJ (2008) Inorg Chem 47:11774
16. Morrissey R, Rodriguez-Lorenzo LM, Gross KA (2005) J Mater Sci: Mater Med 16:387
17. Khudolozhkin BO, Urusov VS, Kurash VV (1974) Geokhimiya 7:1081
18. Jiang M, Terra J, Rossi AM, Morales MA, Baggio Saitovitch EM, Ellis DE (2002) Phys Rev B 66:224107
19. X'Pert Highscore Software Vs 2.2e (2007) PANalytical copyright, Almelo, The Netherlands
20. TenHuissen KS, Brown PW (1999) J Am Ceram Soc 82:2813
21. Caroline Victoria E, Gnanam FD (2002) Artif Organs 16:12
22. Mostafa NY (2005) Mater Chem Phys 94:333
23. Riboud PV (1973) Ann Chim 8:381
24. Kannan S, Ferreira JM (2006) Chem Mater 18:198
25. Li Y, Li Y, Deng ZX, Zhuang J, Sun X (2001) Int J Inorg Mater 3:633
26. Wang Y (2006) Mater Lett 60:1484
27. Lopez-Macipe A (1998) Adv Mater 10:49
28. Fowler BO (1974) Inorg Chem 13:207
29. Vagenas N (2003) Talanta 59:831

30. Legodi M (2001) Miner Eng 14:1107
31. Nyquist RA, Kagel RO (1971) Infrared spectra of inorganic compounds. Academic Press, New York
32. Ning OJ (2004) J Mater Sci: Mater Med 15:1227
33. Randhawa S, Sweety K (2000) Bull Mater Sci 23:305
34. Shaula BAL, Pivak YV, Waerenborgh JC, Gaczyñski P, Yaremchenko AA, Kharton VV (2006) Solid State Ionics 177:2923
35. Russo U, Lovisetto B, Marson S, Speghini A, Bettinelli M (2001) Philos Mag B 81:313
36. Benarafa A (2000) Mater Res Bull 35:2047
37. Ok HN (1969) Phys Rev 185:477
38. Ivanova TI, Frank-Kamenetskaya OV, Kol'tsov AB, Ugolkov V (2001) J Solid State Chem 160:340
39. Low HR, Ritter C, White TJ (2010) Dalton Trans 39:6488